Materials Science & Engineering A 865 (2023) 144659

Contents lists available at ScienceDirect

Materials Science & Engineering A

journal homepage: www.elsevier.com/locate/msea

Effects of strain rate and adiabatic heating on mechanical behavior of medium manganese Q&P steels

Veera Langi *, Guilherme Corrêa Soares, Shahroz Ahmed, Pasi Peura, Mikko Hokka

Tampere University, Materials Science and Environmental Engineering, Tampere, Finland

ARTICLE INFO

Keywords:
Q&P steels
Adiabatic heating
High strain rate
Tensile testing
Multiphase steels
Taylor-Quinney coefficient

ABSTRACT

In this work, the mechanical behavior and properties of four different multiphase steels was studied in tension at strain rates of 10^{-4}, 10^{-2}, 0.5 and 800 s^{-1}. The four materials include a medium manganese (3%) steel grade overcritically and intercritically annealed and Q&P heat treated and two industrially produced TRIP-assisted steels, DH800 and TRIP700 steels, which have different retained austenite morphology. The temperature and strain of the specimens were studied using high speed infrared thermography (IRT) and digital image correlation (DIC). The mechanical response of the Q&P steels had considerably higher tensile strength than the two industrially produced steels. The Q&P steel with a higher austenite volume fraction strain hardened significantly more than the other steels. The DH800 steel and the intercritically annealed Q&P steel heated less with ΔT of 25 °C during uniform deformation than the TRIP700 steel and the overcritically annealed Q&P steel with ΔT of 35 °C. However, the industrially produced steels DH800 and TRIP700 had higher uniform elongation of 0.12 mm/mm and 0.14 mm/mm whereas the Q&P steels reached only 0.09 mm/mm, meaning that the heating rate of the Q&P steels was considerably steeper. In addition, the stronger necking of the DH800 and TRIP700 steels led to much higher maximum temperatures before failure (max. 260 °C) than those observed for the Q&P steels (max. 140 °C). The Taylor-Quinney coefficients of the Q&P steels were large in the beginning of the plastic deformation (0.65–0.95) but decreased as a function of plastic deformation, whereas the Taylor–Quinney Coefficients of the DH800 and TRIP700 steels were lower (0.5–0.6) but increased gradually as a function of plastic deformation.

1. Introduction

The mechanical behavior and properties of metastable austenite containing modern multiphase steels depend strongly on their microstructure but also on strain rate and adiabatic heating, which influence the stability of austenite and the rate of strain induced phase transformations. The mechanical response of these materials has been extensively investigated, but the complexity of the physical and chemical processes governing the microscopic and global mechanical response is difficult to describe in detail. For example, the stability of austenite plays a fundamental role and influences many properties of these steels, including their strength, plasticity, and ductility, but also influences their strain rate sensitivity. Higher strain rate sensitivity is preferred in various energy absorbing automotive applications as it improves the impact performance of the steel.

As the multiphase steels, especially the TRIP assisted steels, are used in various applications in the automotive industry, it is not therefore surprising that the high strain rate properties of these materials have been studied extensively in the past decades. A good comparison of dual phase and TRIP assisted steel with comparable strength levels can be found in the works of Curtze et al. [1] and Hokka et al. [2]. In both studies it was concluded that the strain hardening rate of the austenite containing TRIP steel was strongly dependent on the test temperature, whereas the hardening rate of DP steel with rather similar chemical composition, but no residual austenite, was essentially strain rate independent. As the strain hardening rate is proportional to the rate at which the microstructure of the metal is changing, whereas the current value of the flow stress is proportional to the current state of the microstructure, one can deduce that the microstructure evolution of the TRIP steel was strongly strain rate dependent.

These prior mentioned studies along with several other works [3–5] have indicated that steels where transformation induced plasticity occurs, such as Q&P, TRIP, or metastable austenitic steels have very low or even negative strain rate sensitivities at room temperature. The phase

* Corresponding author.
E-mail address: veera.langi@tuni.fi (V. Langi).

https://doi.org/10.1016/j.msea.2023.144659
Received 6 January 2023; Accepted 16 January 2023
Available online 18 January 2023

transformation rate reduces at high strain rate due to increased stability of austenite, and therefore at high strain rates the strength of the material can be even lower than the strength at low strain rate where strong martensite formation occurs. In the past, the increased stability of austenite has been attributed to adiabatic heating at high strain rates. According to Rusinek et al. [6], the TRIP1000 steel specimen can heat from room temperature to 250 °C at strain rate of 100 s^{-1}. According to the authors, the phase transformations and the plastic deformation of TRIP1000 steel led to non-negligible heating. They studied the energy stored in the microstructure and came to the conclusion that phase transformation affects the energy conversion ratio, but the more exact determination of the stored energy still needs some further studies. According to Soares et al. [7] the temperature of a TRIP700 steel reaches even 300 °C after necking at the strain rate of 600–900 s^{-1}, where the heating was concentrated in the necking area.

Based on the previous, one can say that higher strain rates typically stabilize the austenite and lower the phase transformation rate which is at least partly due to increasing stacking fault energy caused by the adiabatic heating [1,2,8]. At higher temperatures, the metastable austenite requires more plastic deformation or higher stresses, and starts transforming later at larger plastic strains, which leads to lower strain hardening rate in the beginning of the deformation. However, recent findings add further complexity to understanding the effects of strain rate and adiabatic heating on the phase transformation rate and mechanical response of these materials. The plastic deformation in the microscale is typically heterogeneous even though at macroscale the deformation would be uniform. Pun et al. [9] suggested that such heterogeneous plastic deformation at high strain rate and the plastic work in fully austenitic metastable stainless steel can cause local hot spots, where the plastic deformation and the martensite formation are rapid at first, but then the increasing local temperature stops the phase transformation or the growth of the already nucleated martensite particles in that area. Furthermore, Vazquez-Fernandez et al. [10] studied the same austenitic steel and observed that the strain rate itself can affect the martensitic transformation directly and not just through adiabatic heating. The variant of the formed martensite depends on the phase transformation kinetics which again depend on strain rate. The temperature of the environment has the same effect as adiabatic heating, meaning that the austenite in a multiphase steel is more stable at high temperatures [1].

The mechanical response, adiabatic heating, and the phase stability are also strongly affected by the microstructure and the chemical composition of these multiphase steels. For example, the carbon and manganese content affect the mechanical stability [11–13], and especially the thermal stability of austenite [12,13]. During quenching and partitioning heat treatment, the carbon enrichment stabilizes the austenitic phase before quenching to room temperature [14,15]. Higher carbon content also results in improved mechanical stability of austenite [16] and added boron increases the volume fraction of retained austenite, and optimizes its morphology in Q&P steels [17].

The adiabatic heating of the steel is influenced by the original microstructure [18]. The plastic deformation generates plastic work which is partly converted to heat. At high strain rates this heat does not have enough time to dissipate into the surroundings. The part of the plastic work that is not converted to heat is stored in the microstructure as permanent changes in the lattice, dislocations, vacancies etc. The ratio of the heat increment and the plastic work increment is typically called the Taylor-Quinney coefficient [19,20]. The value of the Taylor-Quinney coefficient varies between zero and one for materials where no sources of heat other than the plastic work exist. However, for TRIP steels the exothermic phase transformation also releases heat, which needs to be taken into account when considering the energy balance. However, the main conclusion is that for very stable microstructures most of the mechanical work is converted to heat, whereas a rapidly evolving microstructure can consume more of the energy as permanent changes in the microstructure. Therefore, the original microstructure and the rate at which it evolves during deformation have a strong influence on the final amount of heat that is released during high rate deformation. The heating on the other hand again influences the stability of austenite, and the overall mechanical performance of these steels.

The microstructures of Q&P steels, for example, are very complex and affected strongly by various processing parameters. The temperatures and times affect considerably the microstructure by changing the size, morphology and distribution of the retained austenite [21,22]. Other thermomechanical treatments, for example, cold/hot rolling, also affect the mechanical properties, performance, and the stability of austenite [23]. Cold rolling changes the morphology of retained austenite after the annealing by decreasing the grain size and affects the mechanical properties by increasing tensile strength and ductility when compared to non-cold rolled steel. Pre-quenching of the Q&P steels can increase the total elongation and tensile properties of the steel, and also increase volume fraction of retained austenite [24].

The mechanical properties as well as the stability of the austenite are also affected by the grain size [11,25] and the morphology [26,27]. Wang et al. [28] concluded that smaller grains are less stable against transformation since they have less in-grain deformation substructures that stabilize the grains. On the contrary, De Knijf et al. [29] concluded that smaller grains are more stable and contribute the most to the transformation induced plasticity of the Q&P steel they studied. Blondé et al. [11] came to the similar conclusions with their in-situ experiments. In addition, more nodular austenite has been found more stable than the lath-like austenite. Film-like austenite also seems to be more stable during deformation than blocky austenite [30].

Despite all previous efforts, due the complexity of the microstructure and the mechanical response of these materials, the exact effects of strain rate and adiabatic heating on the mechanical response and the TRIP effect remain partly unknown. In this paper, the effects of original microstructure and retained austenite content on mechanical behavior and adiabatic heating were studied at different strain rates using mechanical testing, high speed photography and infrared thermography. Four steels with different volume fractions of retained austenite and different austenite morphology were tested. The results show that higher original volume fraction of austenite increases the strain hardening during tensile testing. The apparent Taylor-Quinney coefficient is also calculated for these steels. The Taylor-Quinney coefficient provides a quantitative tool for comparison of the energy conversion of different steels during high rate deformation.

2. Materials and methods

Four different steels provided by SSAB Europe Oy were studied in this work. The materials included 800DH and TRIP700 steels which are industrially produced TRIP-assisted steel with a different austenite morphology, as well as a medium manganese steel which was heat treated with two different quenching and partitioning (Q&P) treatments. The TRIP700 was tested only at the highest strain rate as its mechanical properties and performance are well characterized in our previous publications [1,2].

The chemical compositions of the studied steels are presented in Tables 1–3. The Q&P steels were cold rolled medium manganese and low carbon steels. The low carbon and medium manganese content lower the martensite-start temperature and increase the stability of austenite. Silicon and aluminum are added to reduce the carbide

Table 1
The chemical composition of the DH800 steel.

Element	C	Mn	Al	Ni	Ti + Nb + V	Si + Cr + Mo	Balance
DH800	0.16	2.1	0.83	0.05	0.021	0.59	Fe and traces of Cu, P, S

Table 2
The chemical composition of the Q&P steels.

Element	C	Mn	Si + Al	Mo + Cr	Nb	Cu	B	Balance
Q&P	0.26	3.01	2.19	0.43	0.042	0.01	0.005	Fe

Table 3
The chemical composition of the TRIP700 steel.

Element	C	Si + Cr + Mo	Al + Mn	Balance
TRIP700	0.2	0.4	2.9	Fe

formation; however, the silicon content of the steel was limited to avoid hot dip galvanizing problems and aluminum content was increased to compensate for the reduced silicon. Molybdenum and Niobium were added to increase the strength. Niobium also reduces the grain size, whereas boron was added to improve hardenability. The steel was cast into ingot and austenitized at 1250–1300 °C for 2 h. After the austenitization, the steel was hot-rolled to 2.8–3.0 mm thickness at 880 °C and slowly cooled down to room temperature. The steel was then cold rolled into the final thickness of 1.7–1.8 mm. Rectangles or blanks with the length of 75 mm and width of 30 mm were cut from the sheets, and two different Q&P heat treatments were designed, as explained later, and used for processing of the cold rolled blanks to produce two different microstructures. After the heat treatments, the blanks were machined into dog bone samples as shown in Fig. 1. DH800 and TRIP700 steels were tested in the as received condition, and the samples were laser cut from the sheets that of 1.9–2.0 mm thick.

The sample geometry for DH800 and the Q&P steels is shown in Fig. 1. However, the TRIP700 samples had a gage length of 6 mm instead of 8 mm and a shoulder radius of 1 mm instead of 2 mm.

Quench and partition treatments were conducted after full austenitization (also mentioned as overcritical annealing in the text) as well as after intercritical annealing. Speer's model [31,32] was used to calculate the optimum quench temperature for overcritical and intercritical annealed samples to achieve the target austenite volume fraction. Fig. 2 shows the Q&P heat treatment cycles for the overcritical and intercritical annealed samples. Several samples were heat treated with the same parameters. The A_1 and A_3 temperatures, phase fraction of austenite and the composition of the austenite at intercritical annealing temperature were calculated using CALPHAD software JMaTPro (version 12.4).

The volume fractions of retained austenite presented in Table 4 were determined as an average of four measurements measured from two

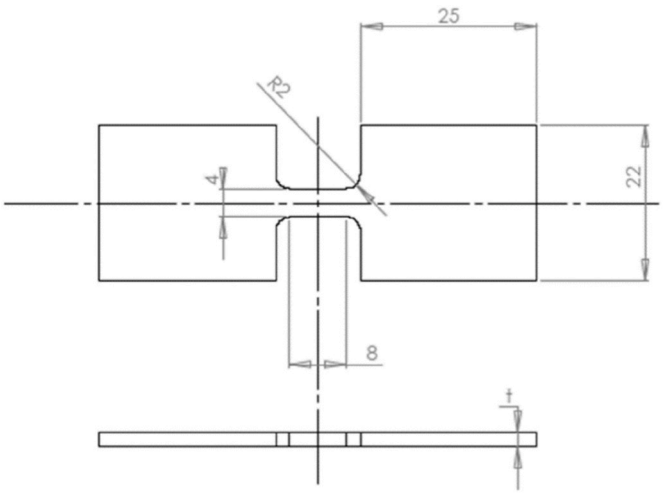

Fig. 1. The sample geometry. Units in mm.

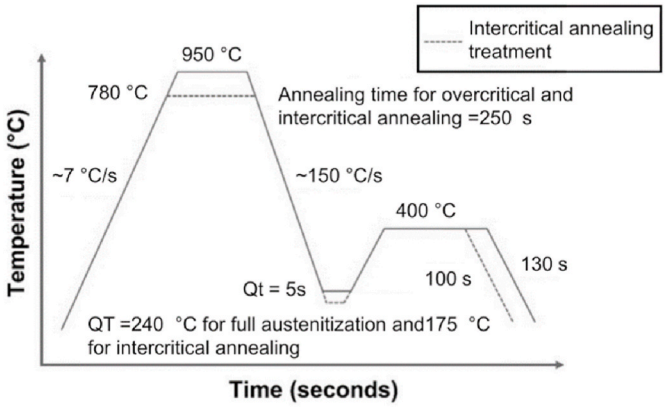

Fig. 2. Heat treatment cycles for the Q&P steels.

Table 4
Volume fraction of the retained austenite of the studied steels.

	DH800	Q&P_IC	Q&P_OC	TRIP700
Retained austenite (%)	12.6 ± 1.1	17.0 ± 2.5	6.7 ± 0.6	19.4 ± 2.7

different samples for each material with the following methods: SAE [33], Miller [34], ASTM [35], Deshayes [36] and Cullity [37]. The average value and the standard deviation were calculated from all measured results. The measurements of the volume fraction of the retained austenite were carried out with Panalytical Empyrean Multipurpose X-ray Diffractometer with Fe-filtered Co-Kα radiation.

Fig. 3 shows scanning electron microscope (SEM) images of the studied steels. The microstructures of DH800, Q&P_OC, and TRIP700 look rather similar to each other. However, the austenite grains in TRIP700 are much larger than in the other more modern steels that were studied. The modern multiphase steels have typically a finer grain size, and the austenite in particular is almost invisible in the SEM micrographs at this magnification. The austenite typically is located as fine sheets between other grains [38,39]. The Q&P_IC and TRIP700 steels have the largest volume fractions of austenite, whereas the Q&P_OC has the least amount of retained austenite. The microstructure of the Q&P steels have more martensite than the other materials. The microstructure of the Q&P_OC (Fig. 3c) is clearly different than the other studied steels as it contains larger quantities of low carbon martensite.

2.1. Mechanical testing

Uniaxial tensile tests were performed at strain rates 10^{-4} s^{-1}, 10^{-2} s^{-1}, 0.5 s^{-1} and 800 s^{-1}. The low strain rate tests up to strain rate of 0.5 s^{-1} were carried out with a servohydraulic Instron 8800 testing device and the high strain rate tests at 800 s^{-1} were performed with a Split Hopkinson Tensile Bar device. The test setups are shown in Fig. 4.

2.2. Full field measurements

The temperature and deformation of the samples were measured during the mechanical loading. At low strain rates the optical images were recorded by two M-Lite 16 Mpix CMOS cameras and at the strain rate of 800 s^{-1}, two Photron SA-X2 high-speed cameras were used. A commercial Digital Image Correlation (DIC) software (LaVision, Davis

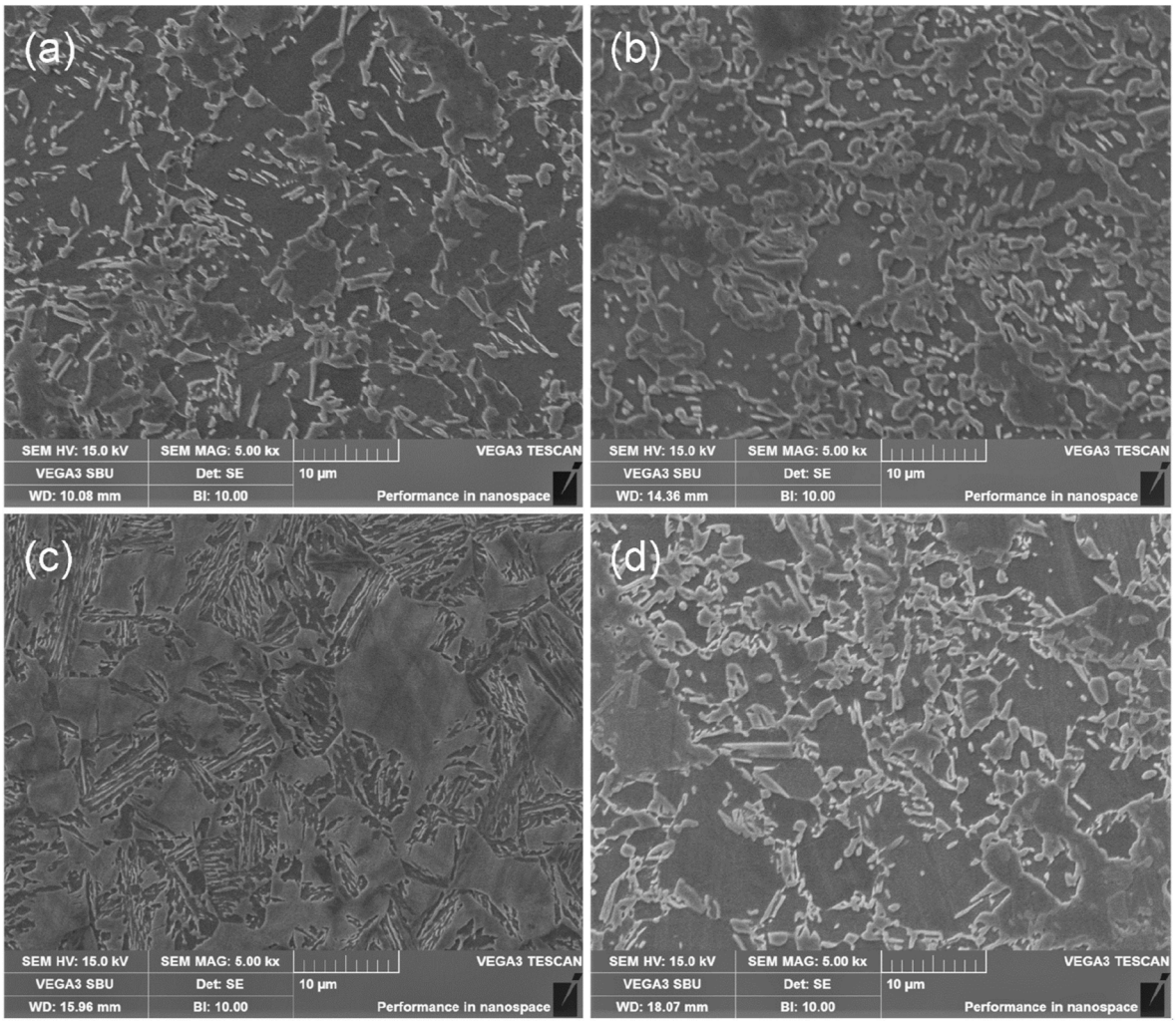

Fig. 3. The microstructures of a) DH800, b) Q&P_IC, c) Q&P_OC and d) TRIP700.

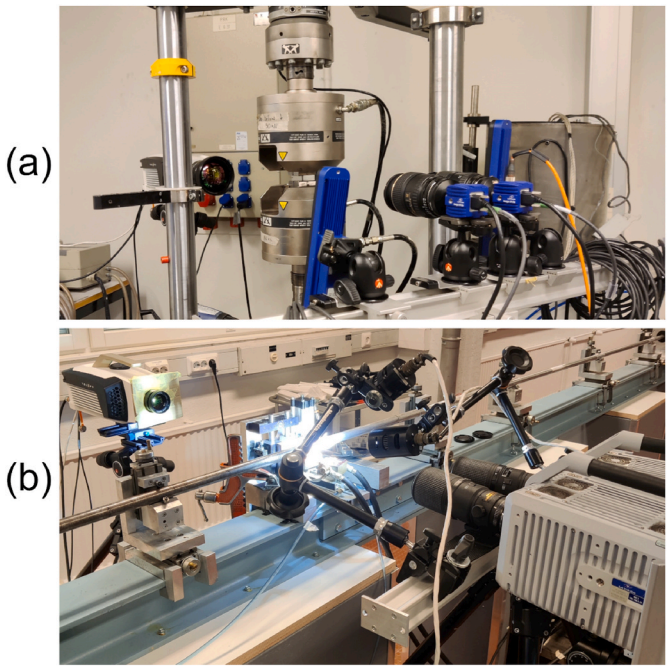

Fig. 4. The test setups for a) low and b) high strain rate testing.

10) was used to calculate the full strain fields from the images. The samples were patterned with black speckles on white background with spray paint. Thermal images were obtained from the other (unpainted) surface with a Telops Fast-IR-M2K camera at all strain rates. The radiometric temperatures obtained by the infrared camera were calibrated by measuring the temperature of a (dummy) specimen with the thermal camera and a K-type thermocouple while the specimen was heated from room temperature up to 200–250 °C. For details about the calibration procedure and the simultaneous temperature and deformation measurements see Ref. [40].

3. Results and discussion

Fig. 5 shows the tensile stress-strain curves of the studied materials at different strain rates. The tensile strength of DH800 increases with increasing strain rate.

At the lowest strain rate of 10^{-4} s^{-1} the yield stress is 550 MPa, as shown in Fig. 5d. At the lowest strain rate, the ultimate tensile strength is 900 MPa and the uniform elongation is 14%. At the strain rate of 10^{-2} s^{-1} the yield stress is increased to 600 MPa and the ultimate tensile strength to 930 MPa, whereas the uniform elongation is at 13%. The behavior of the material is similar at the strain rate of 10^{-2} s^{-1} having the same yield stress of 600 MPa and the ultimate tensile strength of 940 MPa and the main difference is the uniform elongation which is 11%. At the highest strain rate of 800 s^{-1}, the yield stress is 700 MPa, the ultimate tensile strength is 950 MPa and the uniform elongation is 14%.

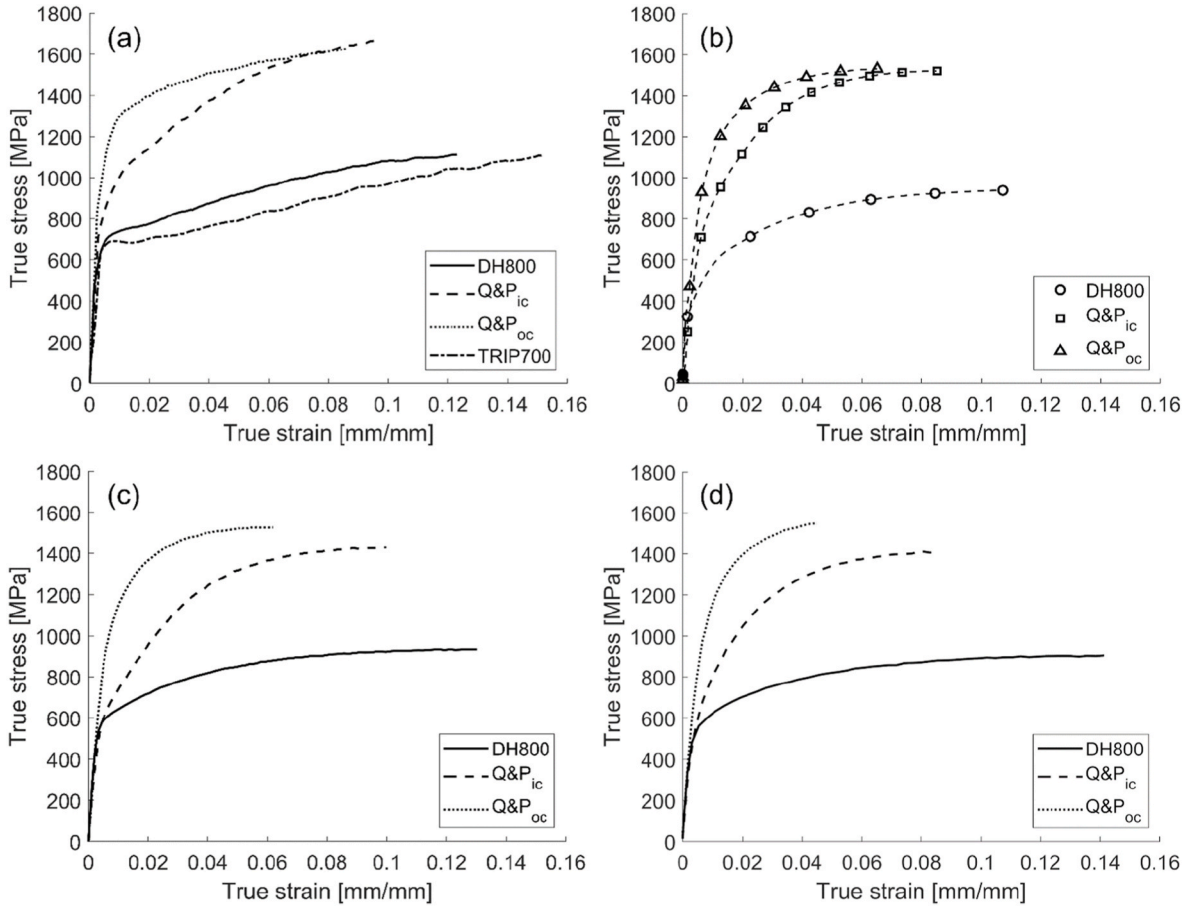

Fig. 5. Stress strain curves at a) 800 s^{-1}, b) 0.5 s^{-1}, c) 10^{-2} s^{-1} and d) 10^{-4} s^{-1}.

While both the yield stress and ultimate tensile strength increase with increasing strain rate, the uniform elongation is not affected as much by the strain rate but is rather similar at all strain rates except for the strain rate of 0.5 s^{-1}, at which it is lower than at the other strain rates. This observation, however, may also be partly due to the poor temporal resolution of the strain measurement at the strain rate of 0.5 s^{-1}.

The strength of the Q&P_IC steel also increases with increasing strain rate, as seen in Fig. 5. At the strain rate of 10^{-4} s^{-1} the yield stress is 640 MPa, ultimate tensile strength is 1410 MPa, and uniform elongation is 8.5%. The corresponding values at the strain rate of 10^{-2} s^{-1} are 650 MPa, 1430 MPa and 10%, whereas at the strain rate of 0.5 s^{-1} the yield stress is 690 MPa and ultimate tensile strength and uniform elongation are 1520 MPa and 8.5%. The yield stress is 850 MPa at the highest strain rate of 800 s^{-1} while the ultimate tensile strength is 1500 MPa and the uniform elongation is 11%. At the lowest strain rate, no necking occurs and the fracture is brittle. At higher strain rates, the ductility is improved and some necking occurs, but not as much as for the DH800 and TRIP700 steels.

Similarly to the previous two steels, the uniform deformation and overall ductility of the Q&P_OC steel increase with increasing strain rate as was also observed for the Q&P_IC steel. At all three lowest strain rates, 10−4 s^{-1}, 10^{-2} s^{-1} and 0.5 s^{-1}, the yield stress is 1100 MPa and the ultimate tensile strength is 1530 MPa. The main difference is in the uniform elongations at different quasi-static strain rates, which are 4.5%, 6.5% and 6.5%, respectively. At the highest strain rate of 800 s^{-1}, the yield stress of Q&P_OC steel is 1300 MPa, ultimate tensile strength is 1480 MPa, and the uniform elongation 9.8%. Also, similarly as what was observed for the Q&P_IC steel, the fracture of the Q&P_OC steel specimens is brittle with no necking at the lowest strain rate, but some necking occurs at the higher strain rates.

The Q&P_IC and Q&P_OC steels have quite similar ultimate tensile strength at different strain rates but the yield stress of the intercritical heat treated steel is considerably lower. This indicates that the Q&P_IC steel strain hardens significantly more than the Q&P_OC steel. This is also visible in the slopes of the stress-strain plots in Fig. 5. The DH800 and the TRIP700 steels have considerably lower yield strength and ultimate tensile strength than the Q&P steels. TRIP700 steel was only tested at the highest strain rate. At 800 s^{-1}, the TRIP700 steel has the yield stress of 680 MPa, ultimate tensile strength of 800 MPa and uniform elongation of 16%, and the overall hardening behavior at this strain rate is comparable to the behavior observed for DH800 steel.

The two Q&P steels have considerably higher strength than the DH800 and TRIP700 steels, as shown in Fig. 5. This is mostly due to larger volume fraction of low carbon martensite in the original undeformed microstructure of the Q&P steels. The Q&P_OC steel has higher yield strength than the Q&P_IC steel at every strain rate, but the Q&P_IC steel strain hardens considerably more especially at the higher strain rates that its ultimate tensile strengths are similar to Q&P_OC. The higher yield strength of Q&P_OC is caused by the high volume fraction of low carbon martensite in the microstructure, which is seen in Fig. 3. The strain hardening of Q&P_IC, on the other hand is at least partly due to the extensive TRIP effect caused by the high amount of austenite transforming into stronger martensite. The TRIP700 and DH800 steels behave similarly to each other with small exceptions in the strength. They have considerably lower yield stresses and ultimate tensile strengths than the Q&P steels and they both strain harden less than the Q&P_IC steel. The lower yield strength is likely due to the softer phases such as ferrite present in the original microstructure. The hardening behavior of the two steels is very similar as the slopes of the stress-strain curves in Fig. 5 are similar. This is due to both dislocation hardening of

the ferrite and other deforming phases, but also due to the gradually proceeding strain induced phase transformation that add strain hardening and improve ductility.

The ductility of the studied Q&P steels enhance as a function of strain rate. At lower strain rates, almost no necking is observed in the samples, but at higher strain rates the samples start to neck. This is clearly observable in the high speed photographs and in the full field strain maps. Increasing uniform elongation with increasing strain rate has been reported for similar medium manganese steels by Yang et al. [41], who explained the observation as due to increase in austenite stability, which is caused by the adiabatic heating and consequent increase in stacking fault energy. The adiabatic heating can also reduce the chemical driving force, thus suppressing the rate of the martensitic transformation [8]. At higher strain rates the rate of phase transformation is slower, and less martensite is formed as the deformation proceeds. This means that there is more austenite available even at larger plastic strains, making the material more ductile and more capable of producing martensite even at these larger strains prolonging the necking even further. When compared to the deformation at lower strain rates, more or possibly even most of the austenite has already deformed into martensite at smaller strains, and therefore, the added hardening capability is exhausted already at smaller strains, and the maximum elongations remain smaller.

The flow strength of the material as a function of strain rate is shown for yield strength, 0.003 strain, 0.005 strain and at UTS in Fig. 6, and the relative (m_r) and absolute (m_a) strain rate sensitivity values are given in Table 5 and the absolute (m_a) sensitivity values are listed in Table 6.

Table 5
Relative strain rate sensitivity values at different strains.

Material	YS	$\varepsilon = 0.03$ mm/mm	$\varepsilon = 0.05$ mm/mm	At UTS
DH800	0.012	0.006	0.008	0.012
Q&P_IC	0.018	0.005	0.007	0.011
Q&P_OC	0.015	−0.001	0.000	0.003

Table 6
Absolute strain rate sensitivity values at different strains.

Material	YS	$\varepsilon = 0.03$ mm/mm	$\varepsilon = 0.05$ mm/mm	At UTS
DH800	17.1	10.5	15.0	27.8
Q&P_IC	31.4	14.9	20.9	40.6
Q&P_OC	39.3	−3.81	−1.45	12.2
TRIP700	31.9 [42]			11.3 [42]

Overall, the strain rate sensitivities of all studied steels are rather low or even negative. The relative strain rate sensitivities of DH800 and Q&P_IC steels are similar, except at yield strength where Q&P_IC steel has a higher relative strain rate sensitivity, as seen in Table 5. The relative strain rate sensitivity of Q&P_OC steel is between that of DH800 and Q&P_IC steels at YS. After yielding Q&P_OC steel has a considerably lower relative strain rate sensitivity than the other two studied materials, being essentially zero or slightly negative at $\varepsilon = 0.03$ and at $\varepsilon = 0.05$.

Q&P_IC steel has the overall highest absolute strain rate sensitivity of

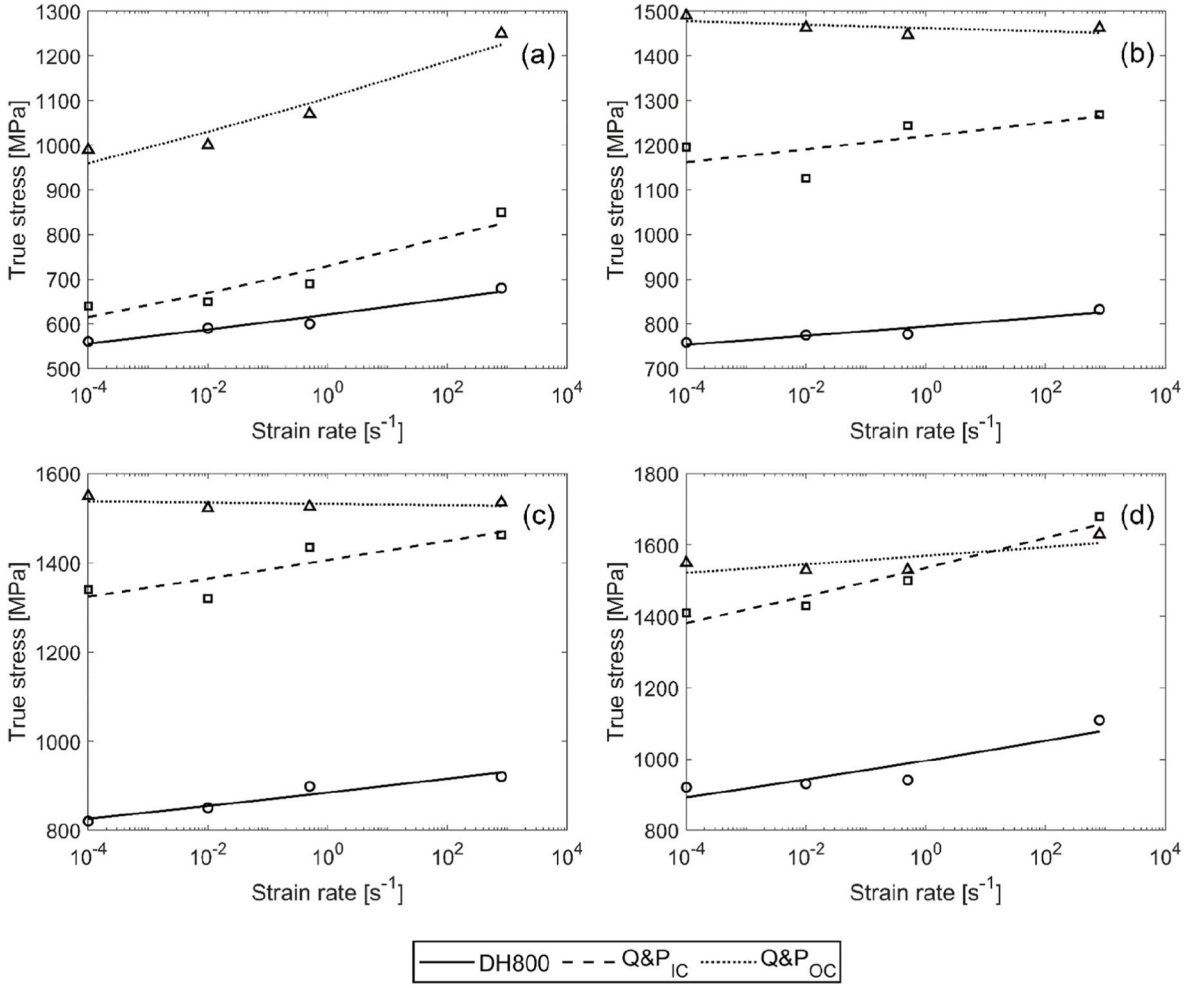

Fig. 6. Relative strain rate sensitivity at a) YS, b) 0.03 mm/mm, c) 0.05 mm/mm and d) at UTS.

the studied materials after yielding, as seen in Table 6. At yield strength, the strain rate sensitivities of Q&P_IC and TRIP700 steels are similar, whereas Q&P_OC steel has a larger absolute strain rate sensitivity, but at UTS the strain rate sensitivity of Q&P_IC steel is the highest when compared to the other studied steels. At $\varepsilon = 0.03$ and at $\varepsilon = 0.05$ the Q&P_OC steel has a small negative strain rate sensitivity and at UTS it behaves similarly to TRIP700.

The data shown in Fig. 6 show some steep upturn behavior, especially for the Q&P steels at small strains (Fig. 6a and b) and for the DH800 steel at UTS (Fig. 6d). The flow stress at the three lowest strain rates seem to align well along a line, but the flow stress at the highest strain rate deviates from this slope. This indicates a change from the thermally activated dislocation motion into more drag controlled region, where such a strong upturn is typically observed. However, such a strong strain rate sensitivity at higher strain rates is not typically observed for austenite containing steels undergoing strain induced phase transformations [1].

Out of the studied materials, the strain sensitivity of the Q&P_OC steel changes the most as plastic deformation proceeds. At yield strength the relative strain rate sensitivity is similar as for the other steels, but with increasing strain, the relative strain rate sensitivity drops essentially to zero and is considerably smaller than those of the other materials. The Q&P_OC steel has the lowest volume fraction of austenite, only $6.7 \pm 0.6\%$, as seen in Table 4, so at higher strains there is less austenite that can transform into martensite to strain harden the metal. In addition, the deformation at yield stress is (quasi-)isothermal, meaning that no adiabatic heating has yet occurred at that point even at higher strain rates. As plastic deformation proceeds, strong adiabatic heating is expected as the strength of the material is remarkably high, and the adiabatic heating is expected to decrease the rate of martensitic transformation.

The negative or very low strain rate sensitivity can be caused by the unstable austenite [1] and the rate effects of the phase transformation rate as explained earlier. In general, the phase transformation rate drops when strain rate is increased. This is at least partly due to the effects of adiabatic heating on the thermodynamic stability of austenite [2]. However, recent studies on TRIP assisted stainless steels [10] have shown that the strain rate itself can also change the kinetics of the phase transformation, and the character or variant of the martensite that forms at low strain rate is different from that observed at high strain rate. Using crystal plasticity simulations, Lindroos et al. [43,44] have recently shown that the adiabatic heating and plastic work can cause local heating in the microstructure of austenitic stainless steels which can lead to formation of 'hot spots' where first martensite forms rapidly, but at the same time this area becomes hotter than its surrounding. The extensive microscopy carried out by Pun et al. [9] indicated that the growth of the martensite stops at those locations. This conclusion cannot directly be applied to multiphase steels, where the austenite is distributed heterogeneously, but the theory can still hold true at least partly. The stability of austenite also in multiphase steels is likely influenced by both strain rate and adiabatic heating in somewhat similar manner as described by Vazquez et al. [10] and Pun et al. [9] for stainless steels, but in multiphase steels the effects can be more difficult due to the complex microstructure as well as the different distribution, size, and morphology of the austenite grains. The strain rate sensitivity of the steels studied in this work is in general rather low, which is not unexpected for such multiphase TRIP-aided steels. However, more work is needed to better understand the true effects of strain rate and adiabatic heating on the phase transformation rate.

The adiabatic heating of the specimens as a function of true strain at strain rates 800 s^{-1} and 0.5 s^{-1} are plotted in Fig. 7 a) and b). The quasi-adiabatic heating at the strain rate of 10^{-2} s^{-1} is plotted in Fig. 7 c). The strain rate of 10^{-2} s^{-1} is called quasi-adiabatic since the strain rate is so low, that some of the heat is conducting from the sample. At the lowest strain rate, 10^{-4}, all the tests were isothermal, and no data is shown here.

The temperatures of the samples shown in Fig. 7 were determined as an average temperature of the whole deforming gauge section. The gauge sections of the samples heat uniformly as long as the deformation is uniform but after the start of necking the heating begins to concentrate on the area of necking. The heat did not conduct to the grip areas of the sample at the two highest strain rates shown in Fig. 7 a) and b). At the strain rate of 10^{-2} s^{-1} some of the heat conducts to the grip areas. The change in the average temperature in Fig. 7 is plotted only until uniform elongation and the data in Fig. 7a were also used to determine the Taylor-Quinney coefficient as will be described later.

The Q&P_OC steel has the highest average temperature change at strain rates 800 s^{-1} and 10^{-2} s^{-1}. At the strain rate 0.5 s^{-1}, Q&P_IC steel has the highest average temperature change at the end of the experiment since it has a higher uniform deformation, but until that point the Q&P_OC steel behaves similarly to the Q&P_IC steel. In this case, as with the stress strain curves, at the poor temporal resolution of the strain measurements at the strain rate of 0.5 s^{-1} needs to be taken into account, and because of this the data points are quite far away from each other, which can lead to higher uncertainty regarding the determination of the uniform elongation at this strain rate, as explained above. DH800 steel has the lowest average temperature change among the studied materials. TRIP700 steel was only tested at the highest strain rate where it behaves similarly as the DH800 steel except that the TRIP700 steel has a higher uniform elongation and therefore it reaches higher average temperature change than the DH800 steel at the end of the uniform elongation.

At the strain rate of 10^{-2} s^{-1}, the heating of the tested materials differs the most from each other. The heating is not quasi-adiabatic, since the heat conducts to the grip areas of the samples. The DH800 steel is measured to only heat up by a few degrees, whereas the Q&P steels heat up significantly more. At this strain rate, also the mechanical response of the materials differs more (Fig. 5c). The strength of the overcritically annealed Q&P_OC steel is much higher than that of the intercritically annealed counterpart. Therefore, it is clear that more mechanical work is produced by the deformation of the stronger material. However, the adiabatic heating is not only affected by the amount

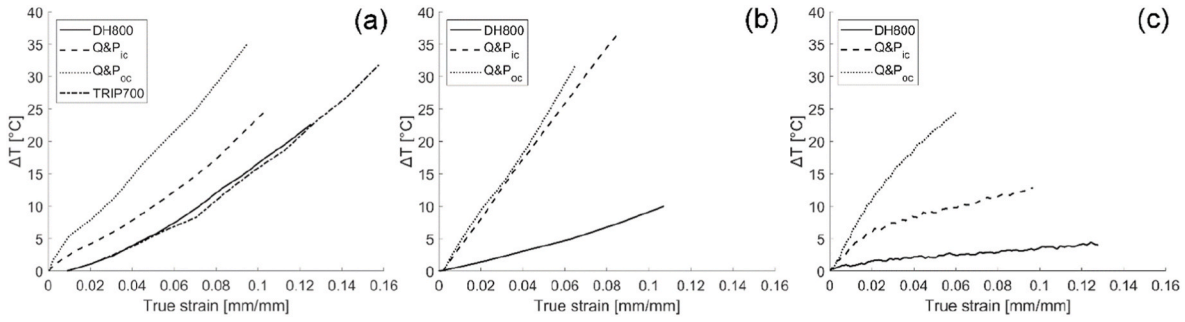

Fig. 7. Change of temperature of the specimen deformed at strain rate a) 800 s^{-1}, b) 0.5 s^{-1} and c) 0.01 s^{-1}.

of mechanical work as will be discussed later.

The maximum temperatures obtained on the surface of the specimen at different strain rates are presented in Fig. 8 as a function of engineering strain. The data include also the temperatures obtained after necking. The maximum temperature of each sample was determined as the temperature of a single point in the gauge section with the highest temperature.

At the highest strain rate, DH800 and TRIP700 steels have the highest maximum temperatures that reach over 260 °C. This is mainly due to the large strains that occur after necking. The Q&P steels, on the other hand, the post uniform elongation is small and similar high temperatures at the strain rate of 800 s^{-1} are not reached. At lower strain rates, the Q&P_OC steel reaches the highest maximum temperatures, followed by Q&P_IC and DH800 steels which have the lowest maximum temperatures at both strain rates of 0.5 and 10^{-2} s^{-1}. Somewhat similar values for the adiabatic heating have been reported by, for example Soares et al. [7] who observed similar maximum temperatures for TRIP700 steel at 600–900 s^{-1} and Rusinek et al. [6] who measured the maximum temperatures of 250 °C for TRIP1000 at strain rate of 100 s^{-1}.

The difference in the strength and ductility of the materials partly explain the difference in the adiabatic heating of the materials during the tensile test. As seen in Fig. 5, the Q&P_OC steel is stronger than Q&P_IC steel. The adiabatic heating in Fig. 8a, for example is very similar for these two studied steels until approximately 20% of engineering strain. However, the stress strain curves in Fig. 5 are different at low plastic strains, but very similar towards the UTS. In fact, at every studied strain rate, the Q&P_OC steel is stronger at small plastic strains but the Q&P_IC steel strain hardens more strongly, and its strength reaches or almost reaches strength of the Q&P_OC steel at UTS. Therefore, it is somewhat unexpected that the adiabatic heating of the two materials is very similar at these strain rates even though the amount of plastic work is different.

The Taylor–Quinney coefficient describes the fraction of the plastic work that is converted into heat during plastic deformation and that which fraction is stored into the microstructure of the material. It can be calculated as the total converted energy converted (β_{int}) or the based on the rate of energy conversion (β_{diff}), i.e., as mechanical power and heating power. In this paper, we used the total converted energy to describe the energy conversion rate in the studied steels. The apparent Taylor–Quinney coefficients (β^a_{int}) includes the latent heat (ΔH) generated by the exothermic phase transformation. For more details and complete derivation of the following equations please refer to Ref. [45]. The apparent Taylor–Quinney coefficient was obtained at the strain rate of 800 s^{-1} and the data are plotted as a function of true plastic strain in Fig. 9. The values were calculated using Equation (1).

$$\beta^a_{int} = \frac{\rho C_p \Delta T}{\int dW_p} \tag{1}$$

where β^a_{int} is the apparent Taylor–Quinney coefficient, ρ is the density of the material (7.80 g/cm3), C_p is the specific heat capacity of the material and dW_p is the mechanical work increment and the ΔT is the temperature change. The specific heat capacity of the DH800 steel was measured as 0.46 J/gK. As the chemical composition of the TRIP700 steel is similar the same specific heat capacity was used for TRIP700. For the Q&P steels, the specific heat capacity of a steel with a similar chemical composition was obtained from literature and it was calculated to be 0.32 J/gK [46].

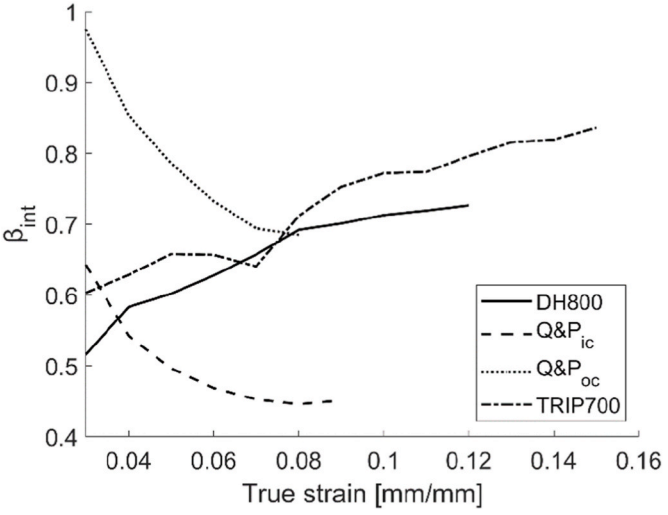

Fig. 9. Apparent Taylor–Quinney coefficient as a function of true strain for the studied steels at the strain rate of 800 s^{-1}.

In the beginning of plastic deformation, the apparent Taylor–Quinney coefficient of the Q&P steels are rather high and then decrease with increasing strain. For Q&P_IC steel the apparent Taylor–Quinney coefficient is close to 0.65 at the beginning of the experiment and for the Q&P_OC steel the values in the beginning of the deformation are above 0.95. For both Q&P steels the Taylor–Quinney coefficient decreases with plastic strain. This means that in the beginning of the plastic deformation a larger fraction of the mechanical energy is converted into heat and at larger plastic strains the conversion of mechanical energy into heat slows down and more energy is stored in the microstructure. This can at least partly be explained by the strength of these steels as each plastic strain increment produces large quantities of mechanical energy. The strength of the steels is mostly due to the larger quantities of low carbon martensite already present in the microstructure (Fig. 3c). However, as the steels include also metastable austenite which is continuously converting into martensite and releasing more heat, it is not so straightforward to interpret how much energy is stored into the microstructure. This overall behavior is also visible in the stress strain plots in Fig. 5, where the strain hardening rate of the Q&P_OC steel is very low, which indicates a microstructure that does not evolve strongly, but is rather stable. The quantitative conclusions of microstructure evolution based on the hardening behavior and the Taylor-Quinney coefficient are similar.

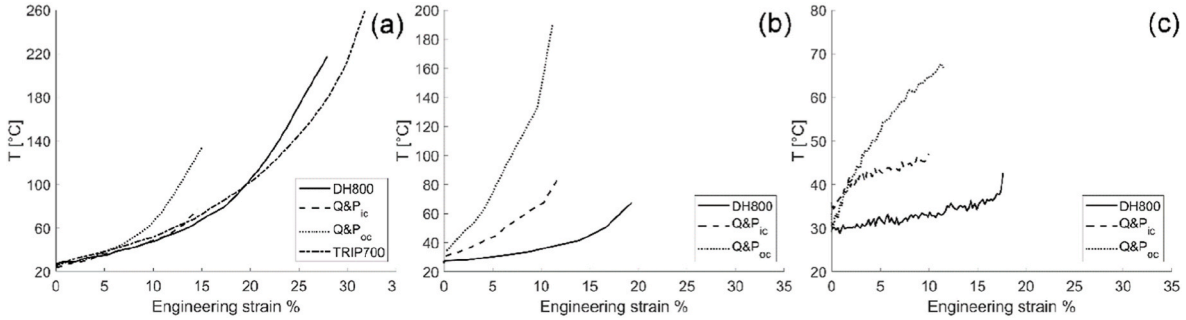

Fig. 8. Maximum temperature of the specimen at strain rate a) 800 s^{-1}, b) 0.5 s^{-1} and c) 0.01 s^{-1}.

Talonen [8] studied a stable and a metastable austenitic stainless steels. The adiabatic heating of the metastable steel was measured to be approximately double when compared to the stable steel. This means that a considerably portion, in his case half, of the total adiabatic heating of steels was caused by the martensitic phase transformation. The strength of the material and the austenite volume fraction also affect the phase transformation enthalpy. The metastable austenitic stainless steels have a fully austenitic microstructure which fully converts to martensite, so the added heat due to the exothermic reaction is much stronger than in multiphase steels containing only a fraction of metastable austenite. For example in this study, the steels contain between 6.7% and 19.4% of austenite, and therefore the potential heat release is smaller than that in fully austenitic steels. The heat release can still be significant and should be evaluated more carefully while taking into account in the energy balance calculations and interpretations of the obtained Taylor-Quinney coefficient.

The DH800 and the TRIP700 steels, on the other hand, behave quite differently compared to the Q&P steels. The apparent Taylor–Quinney Coefficient of DH800 and TRIP700 steels increase with increasing deformation, meaning that more mechanical energy is converted into heat as the deformation proceeds. This clearly means that at early strains the microstructure of the steels is changing more rapidly as energy is rather being stored in the structure than converted to heat. Towards end of the experiment, the microstructure saturates, and more mechanical energy is converted to heat. As seen in Fig. 3, the microstructures of DH800 and TRIP700 steels are quite similar, the mechanical response in Fig. 5a is similar, and finally the apparent Taylor–Quinney-coefficients at different strains are also similar. The strain hardening rate of these two steels is also rather similar. Based on these observations, especially concerning the strain hardening rate and the Taylor-Quinney coefficient it can be concluded that the microstructures of the two steels change in a very similar manner. Both the strain hardening rate and the Taylor-Quinney coefficient describe how fast or how much the microstructure evolves at a given strain, whereas the flow strength of the material is proportional to the current microstructure of the material at the given strain. For the DH800 and TRIP700 steels this conclusion is somewhat surprising as the morphology of the retained austenite is significantly different in these two steels. Especially in the TRIP700 steel the retained austenite islands can be several micrometers and are mostly found in the grain boundaries between ferrite grains, whereas the austenite in DH800 steel is much finer. The smaller retained austenite islands are typically considered more stable [11,47] and should thus transform later during the deformation [48]. This could be expected to lead to different hardening behavior, adiabatic heating and also different Taylor–Quinney coefficients. However, our current observations are only indirect conclusions of the true phase transformation rate and overall microstructure evolution rate, as no *in-situ* measurements of the microstructure are currently available. A measurement of the phase fractions of these steels during high strain rate deformation combined with this current data could reveal much more information and lead to more quantitative description of the evolution of the microstructure and stability of the austenite at different strain rates.

4. Conclusions

- Four different multiphase steels containing retained austenite were studied at four strain rates of 10^{-4}, 10^{-2}, 0.5 and 800 s^{-1}. The steels included industrially produced TRIP-assisted DH800 and TRIP700 steels and a medium manganese steel which was intercritically and overcritically heat annealed before quenching and partitioning heat treatment.
- Stress strain response of the materials differs quite significantly. The Q&P steels had higher strength than the DH800 and TRIP700 steels. The overcritically annealed Q&P_OC steel had higher yield strength than the intercritically annealed Q&P_IC steel at all strain rates, but at UTS the true stress of the materials was similar since Q&P_IC steel strain hardens considerably more. The higher strength of the Q&P_OC steels was due to the large fraction of low carbon martensite in the original microstructure.
- At yield stress both the relative and absolute strain rate sensitivity of all the studied materials are positive with DH800 steel being the least strain rate sensitive and the other materials being quite similar to each other. At strains of 0.03 and 0.05 mm/mm, the strain rate sensitivity of Q&P_OC steel is slightly negative or zero. DH800 and Q&P_IC steels have really similar relative strain rate sensitivities, but the Q&P_IC steel has the overall highest absolute strain rate sensitivity.
- The maximum adiabatic heating was at the strain rate of 800 s^{-1} where the maximum temperatures reached 70–260 °C. The highest temperatures were observed for the DH800 and the TRIP700 steels that showed most post necking plasticity. No strain localizations were observed for the Q&P steels at low strain rates, but some necking was observed at higher strain rates. The overall plasticity of the Q&P steels also increased with strain rate.
- The Taylor-Quinney Coefficients of the Q&P steels were high in the beginning and then decreased gradually with plastic deformation. For the Q&P_IC steel the Taylor-Quinney coefficient was much lower; around 0.65, which indicates a strongly changing microstructure compared to the Q&P_OC steel whose Taylor-Quinney Coefficient was close to 0.95 at the beginning of plastic deformation. Similar qualitative conclusions about the changes in the microstructure were drawn based on the hardening rates of the two materials.
- The Taylor–Quinney Coefficients of the DH800 and the TRIP700 steels were rather low at small plastic strains, but gradually increased with plastic deformation indicating a microstructure that is actively changing in the beginning of the plastic deformation, but gradually stabilizing so that more plastic work is converted to heat and the microstructure is more stable. The energy conversion, strain hardening, strength, and ductility of these two materials are very similar, which is rather surprising considering that the microstructure, and especially the morphology of the retained austenite, are different from each other. It seems, therefore, that the energy conversion ratio and the adiabatic heating of the alloys is not strongly dependent on the morphology of austenite.

CRediT authorship contribution statement

Veera Langi: Conceptualization, Investigation, Data curation, Writing – original draft. **Guilherme Corrêa Soares:** Investigation, Data curation, Writing – review & editing. **Shahroz Ahmed:** Writing – review & editing. **Pasi Peura:** Writing – review & editing. **Mikko Hokka:** Conceptualization, Supervision, Funding acquisition, Writing – review & editing.

Declaration of competing interest

The authors declare that they have no known competing financial interests or personal relationships that could have appeared to influence the work reported in this paper.

Data availability

The data is published online in Zenodo at: https://doi.org/10.5281/zenodo.7544230.

References

[1] S. Curtze, V.T. Kuokkala, M. Hokka, P. Peura, Deformation behavior of TRIP and DP steels in tension at different temperatures over a wide range of strain rates, Mater. Sci. Eng., A 507 (1–2) (May 2009) 124–131, https://doi.org/10.1016/J.MSEA.2008.11.050.

[2] M. Hokka, V.-T. Kuokkala, S. Curtze, Dynamic tensile behaviour of TRIP and DP steels at different temperatures, Steel Res. Int. 80 (2) (Feb. 2009) 137–145, https://doi.org/10.2374/SRI08SP090.

[3] J. van Slycken, P. Verleysen, J. Degrieck, J. Bouquerel, B.C. de Cooman, Dynamic response of aluminium containing TRIP steel and its constituent phases, Mater. Sci. Eng., A 460 (461) (Jul. 2007) 516–524, https://doi.org/10.1016/J.MSEA.2007.01.075.

[4] M. Isakov, Strain Rate History Effects in a Metastable Austenitic Stainless Steel, PhD Thesis, Tampere University of Technology, Tampere, 2012. Oct. 16, 2022. [Online]. Available: https://trepo.tuni.fi/handle/10024/114635.

[5] P. Larour, P. Verleysen, K. Dahmen, W. Bleck, Strain rate sensitivity of pre-strained AISI 301LN2B metastable austenitic stainless steel, Steel Res. Int. 84 (1) (Jan. 2013) 72–88, https://doi.org/10.1002/SRIN.201200120.

[6] A. Rusinek, J.R. Klepaczko, Experiments on heat generated during plastic deformation and stored energy for TRIP steels, Mater. Des. 30 (1) (Jan. 2009) 35–48, https://doi.org/10.1016/j.matdes.2008.04.048.

[7] G.C. Soares, N.I. Vázquez-Fernández, M. Hokka, Thermomechanical behavior of steels in tension studied with synchronized full-field deformation and temperature measurements, Exp. Tech. 45 (5) (Oct. 2021) 627–643, https://doi.org/10.1007/S40799-020-00436-Y/FIGURES/13.

[8] J. Talonen, Effect of Strain-Induced α'-Martensite Transformation on Mechanical Properties of Metastable Austenitic Stainless Steels, PhD DIssertation, Helsinki University of Technology, Espoo, 2007. Oct. 13, 2022. [Online]. Available: http://lib.tkk.fi/Diss/2007/isbn9789512287802/.

[9] L. Pun, G.C. Soares, M. Isakov, M. Hokka, Effects of strain rate on strain-induced martensite nucleation and growth in 301LN metastable austenitic steel, Mater. Sci. Eng., A 831 (Jan. 2022), 142218, https://doi.org/10.1016/J.MSEA.2021.142218.

[10] N.I. Vázquez-Fernández, T. Nyyssönen, M. Isakov, M. Hokka, V.T. Kuokkala, Uncoupling the effects of strain rate and adiabatic heating on strain induced martensitic phase transformations in a metastable austenitic steel, Acta Mater. 176 (Sep. 2019) 134–144, https://doi.org/10.1016/J.ACTAMAT.2019.06.053.

[11] R. Blondé, et al., Mechanical stability of individual austenite grains in TRIP steel studied by synchrotron X-ray diffraction during tensile loading, Mater. Sci. Eng. 618 (Nov. 2014) 280–287, https://doi.org/10.1016/j.msea.2014.09.008.

[12] R.M. Wu, W. Li, C.L. Wang, Y. Xiao, L. Wang, X.J. Jin, Stability of retained austenite through a combined intercritical annealing and quenching and partitioning (IAQP) treatment, Acta Metall. Sin. 28 (3) (Mar. 2015) 386–393, https://doi.org/10.1007/s40195-015-0217-9.

[13] H. Luo, Comments on 'austenite stability of ultrafine-grained transformation-induced plasticity steel with Mn partitioning' by S. Lee, S.J. Lee and B.C. de Cooman, Scripta Mater. 65 (2011) 225–228, https://doi.org/10.1016/j.scriptamat.2012.01.017. Scripta Materialia, vol. 66, no. 10. Elsevier Ltd, pp. 829–831, May 01, 2012.

[14] M.J. Santofimia, L. Zhao, J. Sietsma, Overview of mechanisms involved during the quenching and partitioning process in steels, in: Metallurgical and Materials Transactions A: Physical Metallurgy and Materials Science, 42, Dec. 2011, pp. 3620–3626, https://doi.org/10.1007/s11661-011-0706-z, 12.

[15] J.G. Speer, E. de Moor, A.J. Clarke, Critical assessment 7: quenching and partitioning, Mater. Sci. Technol. 31 (1) (2015) 3–9, https://doi.org/10.1179/1743284714Y.0000000628. Maney Publishing, Jan. 01.

[16] S. Ebner, R. Schnitzer, E. Maawad, C. Suppan, C. Hofer, Influence of partitioning parameters on the mechanical stability of austenite in a Q& P steel: a comparative in-situ study, Materialia (Oxf) 15 (Mar. 2021), 101033, https://doi.org/10.1016/j.mtla.2021.101033.

[17] Z. Li, R. Wu, S. Song, Y. Wang, T. Wu, Influence of changes in alloying elements distribution and retained Austenite (RA) on mechanical properties of high boron alloy during quenching and partitioning(Q&P) process, J. Mater. Res. Technol. 18 (May 2022) 4748–4761, https://doi.org/10.1016/j.jmrt.2022.04.124.

[18] G.C. Soares, M. Hokka, The Taylor–Quinney coefficients and strain hardening of commercially pure titanium, iron, copper, and tin in high rate compression, Int. J. Impact Eng. 156 (Oct. 2021), 103940, https://doi.org/10.1016/J.IJIMPENG.2021.103940.

[19] G.I. Taylor, H. Quinney, The latent energy remaining in a metal after cold working, in: Proceedings of the Royal Society of London. Series A, Containing Papers of a Mathematical and Physical Character 143, Jan. 1934, pp. 307–326, https://doi.org/10.1098/rspa.1934.0004, 849.

[20] W.S. Farren, G.I. Taylor, The heat developed during plastic extension of metals, in: Proceedings of the Royal Society of London. Series A, Containing Papers of a Mathematical and Physical Character 107, Mar. 1925, pp. 422–451, https://doi.org/10.1098/rspa.1925.0034, 743.

[21] I. de Diego-Calderón, et al., Global and local deformation behavior and mechanical properties of individual phases in a quenched and partitioned steel, Mater. Sci. Eng. 630 (Apr. 2015) 27–35, https://doi.org/10.1016/j.msea.2015.01.077.

[22] M.I.T. Tzini, J.S. Aristeidakis, P.I. Christodoulou, A.T. Kermanidis, G. N. Haidemenopoulos, D. Krizan, Multi-phase field modeling in TRIP steels: distributed vs. average stability and strain-induced transformation of retained austenite, Mater. Sci. Eng. 833 (Jan. 2022), https://doi.org/10.1016/j.msea.2021.142341, 142341.

[23] X. Rong, B. Hu, H. Guo, M. Enomoto, C. Shang, Influence of cold rolling on the stability of retained austenite and mechanical properties of a Cu bearing low carbon low manganese steel, Mater. Sci. Eng., A 850 (Aug. 2022), 143455, https://doi.org/10.1016/j.msea.2022.143455.

[24] J. Zhang, H. Ding, R.D.K. Misra, C. Wang, Enhanced stability of retained austenite and consequent work hardening rate through pre-quenching prior to quenching and partitioning in a Q-P microalloyed steel, Mater. Sci. Eng. 611 (Aug. 2014) 252–256, https://doi.org/10.1016/j.msea.2014.05.074.

[25] R.D.K. Misra, V.S.A. Challa, P.K.C. Venkatsurya, Y.F. Shen, M.C. Somani, L. P. Karjalainen, Interplay between grain structure, deformation mechanisms and austenite stability in phase-reversion-induced nanograined/ultrafine-grained austenitic ferrous alloy, Acta Mater. 84 (Feb. 2015) 339–348, https://doi.org/10.1016/j.actamat.2014.10.038.

[26] J. Hidalgo, K.O. Findley, M.J. Santofimia, Thermal and mechanical stability of retained austenite surrounded by martensite with different degrees of tempering, Mater. Sci. Eng. 690 (Apr. 2017) 337–347, https://doi.org/10.1016/j.msea.2017.03.017.

[27] X.C. Xiong, B. Chen, M.X. Huang, J.F. Wang, L. Wang, The effect of morphology on the stability of retained austenite in a quenched and partitioned steel, Scripta Mater. 68 (5) (Mar. 2013) 321–324, https://doi.org/10.1016/j.scriptamat.2012.11.003.

[28] M.M. Wang, C.C. Tasan, D. Ponge, A. Kostka, D. Raabe, Smaller is less stable: size effects on twinning vs. transformation of reverted austenite in TRIP-maraging steels, Acta Mater. 79 (Aug. 2014) 268–281, https://doi.org/10.1016/j.actamat.2014.07.020.

[29] D. de Knijf, C. Föjer, L.A.I. Kestens, R. Petrov, Factors influencing the austenite stability during tensile testing of Quenching and Partitioning steel determined via in-situ Electron Backscatter Diffraction, Mater. Sci. Eng. 638 (Jun. 2015) 219–227, https://doi.org/10.1016/j.msea.2015.04.075.

[30] X.C. Xiong, B. Chen, M.X. Huang, J.F. Wang, L. Wang, The effect of morphology on the stability of retained austenite in a quenched and partitioned steel, Scripta Mater. 68 (5) (Mar. 2013) 321–324, https://doi.org/10.1016/j.scriptamat.2012.11.003.

[31] J.G. Speer, A.M. Streicher, D. Matlock, F. Rizzo, G. Krauss, Quenching and partitioning: a fundamentally new process to create high strength trip sheet microstructures - technische informationsbibliothek (TIB), in: Materials Science and Technology 2003 Meeting, 2003, pp. 505–522. Aug. 10, 2022. [Online]. Available: https://www.tib.eu/en/search/id/BLCP%3ACN050898361/Quenching-and-Partitioning-A-Fundamentally-New/.

[32] J.G. Speer, F.C. Rizzo Assunção, D.K. Matlock, D.v. Edmonds, The 'quenching and partitioning' process: background and recent progress, Mater. Res. 8 (4) (2005) 417–423, https://doi.org/10.1590/S1516-14392005000400010. Universidade Federal de Sao Carlos.

[33] C. Jatczak, J.A. Larson, S.W. Shin, SP-453 Retained Austenite and its Measurement by X-Ray Diffraction, 1980.

[34] R.L. Miller, A rapid X-ray method for the determination of retained austenite, Transactions of the American Society for Metals 57 (1964) 892–899.

[35] ASTM, ASTM E975 Standard Practice for X-Ray Determination of Retained Austenite in Steel with Near Random Crystallographic Orientation, 2013.

[36] P. Deshayes, Consequences du refroidissement acceleré doux après laminage controlé sur la microstructure et les proprietés mecaniques d'aciers à 0.1% de carbone, PhD Thesis, L'Université des Sciences et Technologies de Lille, Lille, 1995.

[37] B.D. Cullity, Elements of X-Ray Diffraction, second ed., Addison-Wesley Publishing Co, Inc., 1978.

[38] O. Oja, Correlation between the Microstructure and Mechanical Properties of Intercritically Annealed Advanced High-Strength Steels, Aug. 2022, p. 184. Oct. 13, 2022. [Online]. Available: https://trepo.tuni.fi/handle/10024/140848.

[39] O. Oja, A. Saastamoinen, M. Patnamsetty, M. Honkanen, P. Peura, M. Järvenpää, Microstructure and mechanical properties of Nb and V microalloyed TRIP-assisted steels, Metals 9 (8) (Aug. 2019) 887, https://doi.org/10.3390/MET9080887, 2019, Vol. 9, Page 887.

[40] G.C. Soares, N.I. Vázquez-Fernández, M. Hokka, Thermomechanical behavior of steels in tension studied with synchronized full-field deformation and temperature measurements, Exp. Tech. 45 (5) (Oct. 2021) 627–643, https://doi.org/10.1007/s40799-020-00436-y.

[41] Y. gang Yang, et al., Effects of strain rate on austenite stability and mechanical properties in a 5Mn steel, J. Iron Steel Res. Int. 29 (2) (Feb. 2022) 316–326, https://doi.org/10.1007/s42243-021-00569-3.

[42] S. Curtze, V.T. Kuokkala, M. Hokka, P. Peura, Deformation behavior of TRIP and DP steels in tension at different temperatures over a wide range of strain rates, Mater. Sci. Eng. 507 (1–2) (May 2009) 124–131, https://doi.org/10.1016/j.msea.2008.11.050.

[43] M. Lindroos, et al., Micromechanical modeling approach to single track deformation, phase transformation and residual stress evolution during selective laser melting using crystal plasticity, Addit. Manuf. 38 (Feb. 2021), 101819, https://doi.org/10.1016/j.addma.2020.101819.

[44] M. Lindroos, M. Isakov, A. Laukkanen, Crystal plasticity modeling of transformation plasticity and adiabatic heating effects of metastable austenitic stainless steels, Int. J. Solid Struct. 236 (237) (Feb. 2022), 111322, https://doi.org/10.1016/j.ijsolstr.2021.111322.

[45] N. Vázquez, Effects of Strain Rate and Adiabatic Heating on the Strain-Induced Martensitic Phase Transformation in Austenitic Stainless Steels, PhD Thesis, Tampere University, Tampere, 2020. Oct. 15, 2022. [Online]. Available: https://trepo.tuni.fi/handle/10024/123511.

[46] A.C. Mitchell, XX.—on the thermal conductivity and specific heat of manganese-steel, Trans. R. Soc. Edinb. 35 (4) (1890) 947–954, https://doi.org/10.1017/S0080456800008577.

[47] D. de Knijf, C. Föjer, L.A.I. Kestens, R. Petrov, Factors influencing the austenite stability during tensile testing of Quenching and Partitioning steel determined via in-situ Electron Backscatter Diffraction, Mater. Sci. Eng. 638 (Jun. 2015) 219–227, https://doi.org/10.1016/j.msea.2015.04.075.

[48] I. Choi, D. Son, S.J. Kim, D.K. Matlock, J.G. Speer, Strain rate effects on mechanical stability of retained austenite in TRIP sheet steels, SAE Technical Papers, J. Mater. Manuf. 115 (Section 5) (2006) 898–910, https://doi.org/10.4271/2006-01-1434.